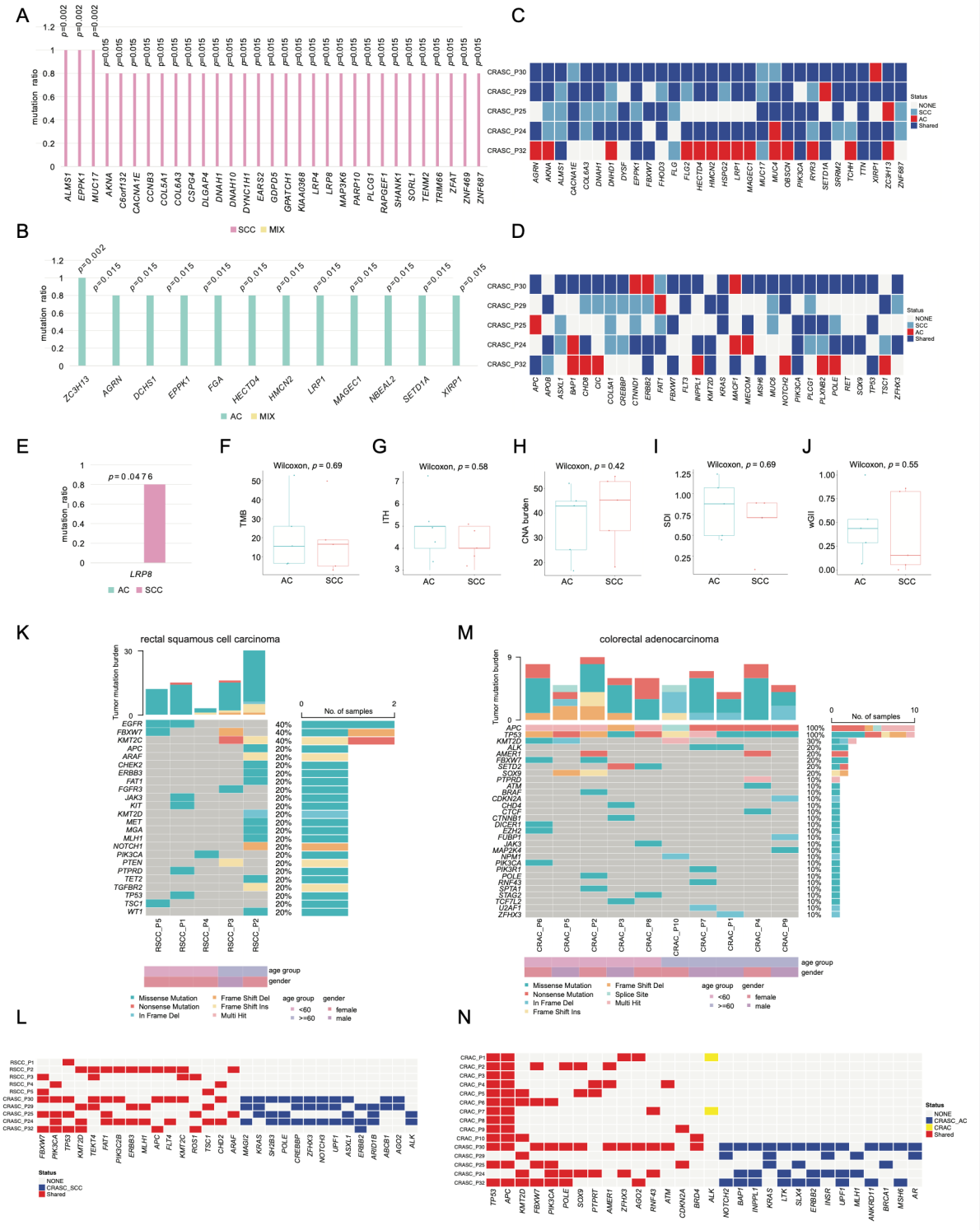

Extended Data Fig. 1 Genomic divergence between adenocarcinoma and squamous cell carcinoma components of CRASC

(A) Bar plot showing mutation ratios of genes enriched in the squamous cell carcinoma (SCC) component relative to mixed samples (MIX group), with genes ordered by mutation ratio.

(B) Bar plot showing mutation ratios of genes enriched in the AC component relative to mixed samples (MIX group), with genes ordered by mutation ratio.

(C) Heatmap summarizing validated somatic mutations across all detected genes in paired SCC and

AC regions from the same patients. Mutation status is classified as SCC-private, AC-private, shared (present in both components), or none (absent).
(D) Heatmap summarizing validated driver gene mutations using the same classification (SCC-private, AC-private, shared, or none) across paired components.
(E) Comparison of LRP8 mutation ratios between SCC and AC components of CRASC.
(F-J) Box-and-whisker plots comparing major genomic features between AC and SCC components of CRASC, including tumor mutational burden (TMB; F), intratumor heterogeneity (ITH; G), copy number alteration (CNA) burden (H), Shannon diversity index (SDI; I), and weighted genome instability index (wGII; J). Boxes indicate the interquartile range (IQR), with the median shown as the center line; whiskers represent the range of the data as plotted. Two-sided Wilcoxon tests were used for group comparisons.
(K) Oncoprint showing somatic mutations in rectal squamous cell carcinoma (RSCC) samples (n = 5).
(L) Heatmap comparing driver gene alteration frequencies between the SCC component of CRASC and RSCC.
(M) Oncoprint showing somatic mutations in colorectal adenocarcinoma (CRAC) samples (n = 10).
(N) Heatmap comparing driver gene alteration frequencies between the AC component of CRASC and CRAC.

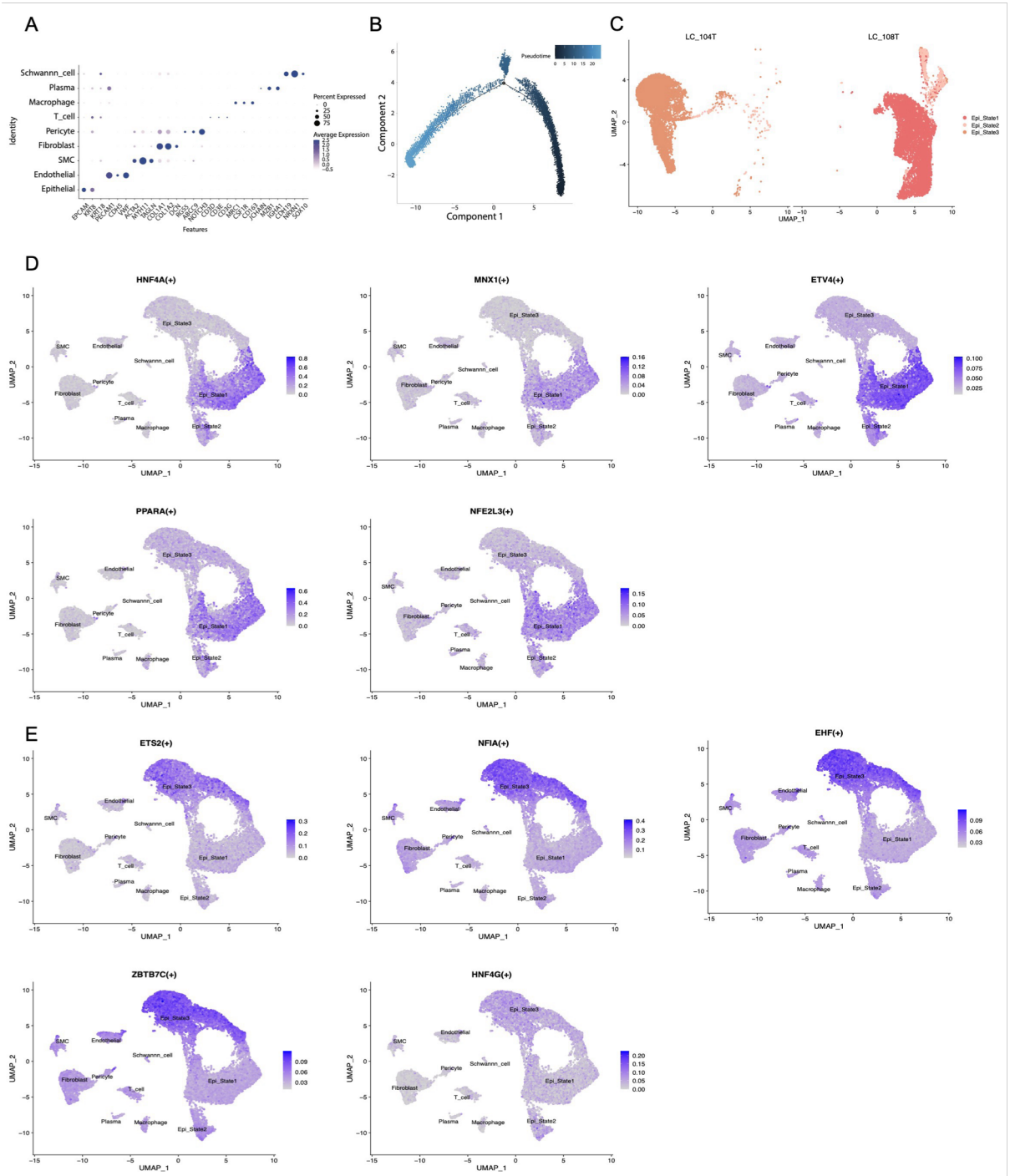

Extended Data Fig. 2 Annotation of cell lineages and characterization of epithelial regulatory landscapes

(A) Dot plot displaying the expression of the marker genes used to annotate major cell types identified in the CRASC samples. Dot size indicates the percentage of cells expressing the gene, while color intensity reflects the average scaled expression level.

(B) Pseudotime trajectory inferred by Monocle2 using the top variable genes. Cells are colored by pseudotime value, with dark blue indicating the starting point and light blue indicating the terminal states.

(C) UMAP visualization of the epithelial subpopulation, with cells from different samples shown separately.

(D-E) UMAP feature plots visualizing the regulon activity scores derived from PySCENIC analysis for

key transcription factors. (D) Transcription factors specifically enriched in Epi_State1, including *HNF4A*, *MNX1*, *ETV4*, *PPARA*, and *NFE2L3*. (E) Transcription factors specifically enriched in Epi_State3, including *ETS2*, *NFIA*, *EHF*, *ZBTB7C*, and *HNF4G*. The color scale represents the regulon specificity score (RSS).

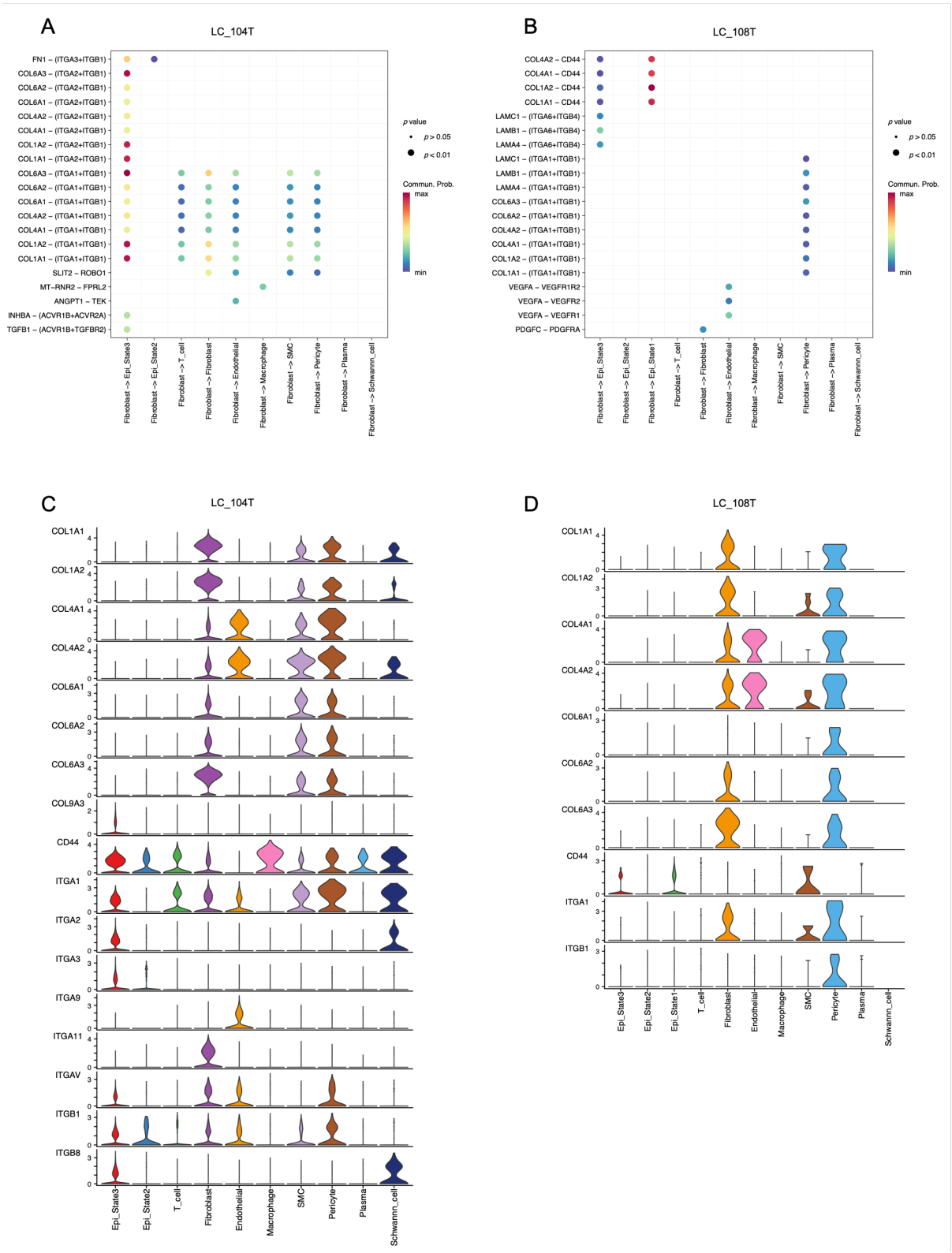

Extended Data Fig. 3 Fibroblast-mediated cell-cell communication networks exhibit distinct patterns between CRASC subtypes

(A-B) Dot plots illustrating significant ligand-receptor interactions originating from fibroblasts to other cell types in sample LC_104T (A) and LC_108T (B), inferred using CellChat. The x-axis represents the target cell populations receiving signals from fibroblasts, while the y-axis displays specific ligand-

receptor pairs. Dot size reflects the statistical significance (P value), and the color gradient indicates the communication probability (interaction strength).
(C-D) Stacked violin plots showing the log-normalized expression levels of key ligand genes (collagens) and receptor genes (integrins and *CD44*) across all identified cell clusters in LC_104T (C) and LC_108T (D).

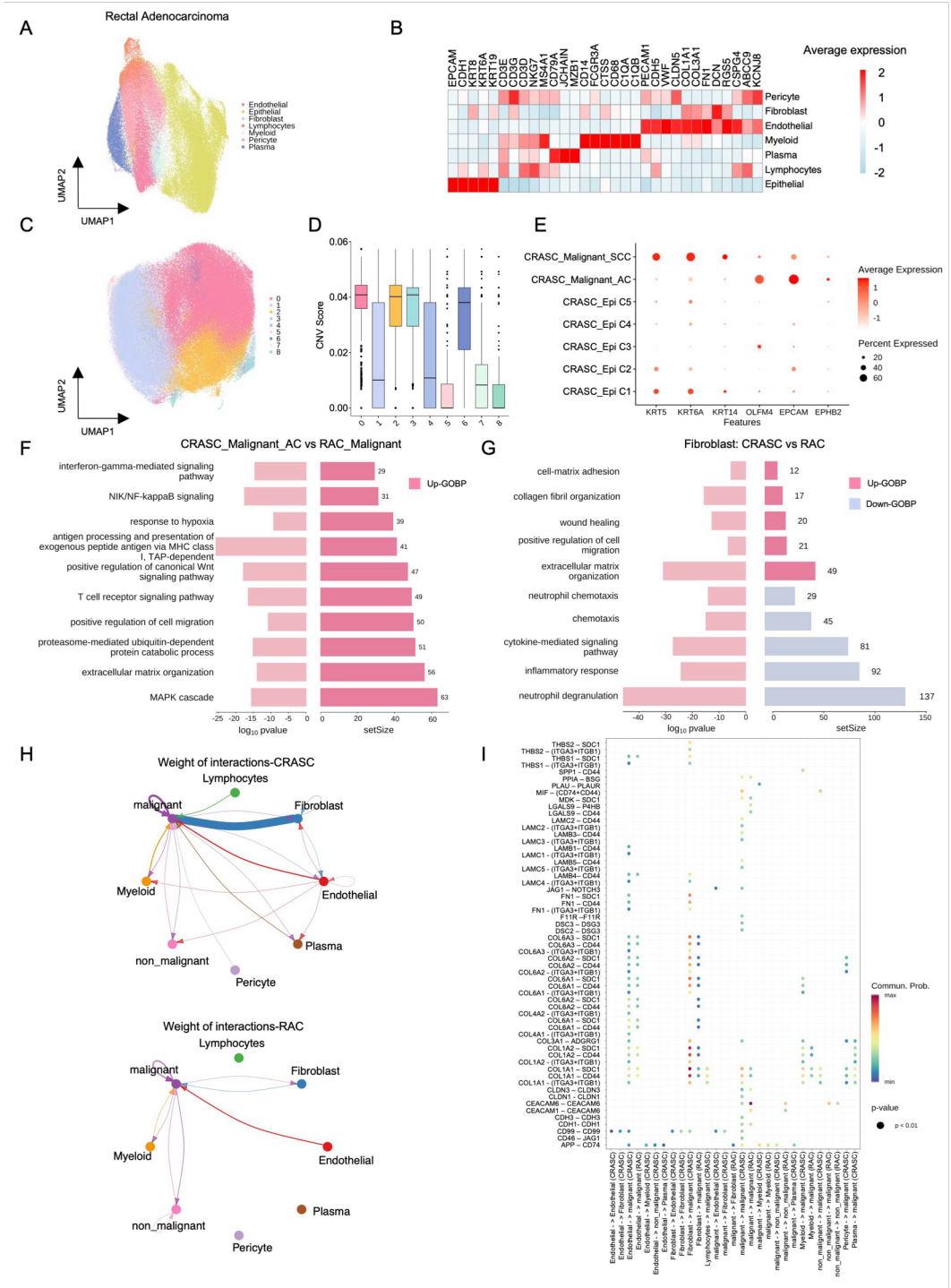

Extended Data Fig. 4 Spatial transcriptomic characterization and comparative analysis of CRASC and RAC

(A) UMAP projection of SMI data from RAC samples, colored by annotated major cell types.

(B) Expression patterns of representative marker genes across the identified cell types.

(C) UMAP visualization of epithelial cells from CRASC samples, colored by transcriptionally defined clusters.

(D) Box plots showing copy number variation (CNV) scores across epithelial clusters.

(E) Dot plot shows marker genes that distinguish epithelial subtypes in CRASC.

(F) GO biological process enrichment analysis of differentially expressed genes between the AC

component of CRASC and the malignant component of RAC.
(G) GO biological process enrichment analysis of genes significantly upregulated and downregulated in fibroblasts from CRASC compared to RAC.
(H) Network visualization depicting the relative interaction weights in CRASC and RAC samples, thicker lines indicate a higher weight of interactions.
(I) Inference of cell-cell communication by comparing ligand-receptor pair-mediated signaling probabilities between CRASC and RAC samples.

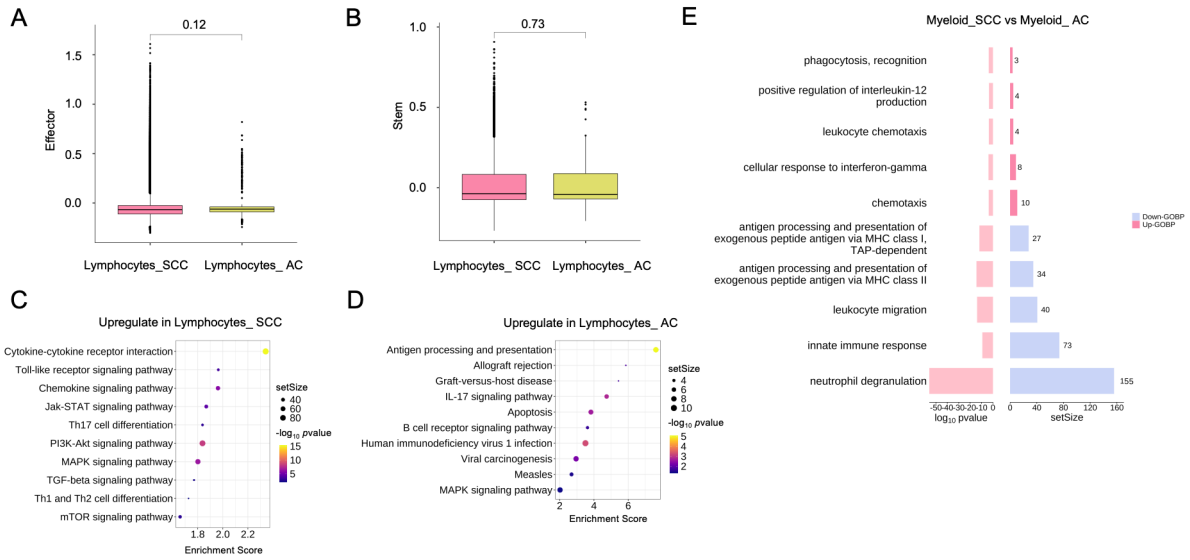

Extended Data Fig. 5 Spatial colocalization patterns and immune functional states in CRASC and RAC

(A-B) Box plots comparing the expression scores of effector- and stemness-associated gene signatures in lymphocytes proximal to CRASC_Malignant_SCC and CRASC_Malignant_AC.

(C) KEGG pathway enrichment analysis of genes significantly upregulated in lymphocytes proximal to CRASC_Malignant_SCC.

(D) KEGG pathway enrichment analysis of genes significantly upregulated in lymphocytes proximal to CRASC_Malignant_AC.

(E) GO biological process enrichment analysis of genes significantly upregulated and downregulated in myeloid_SCC versus myeloid_AC.

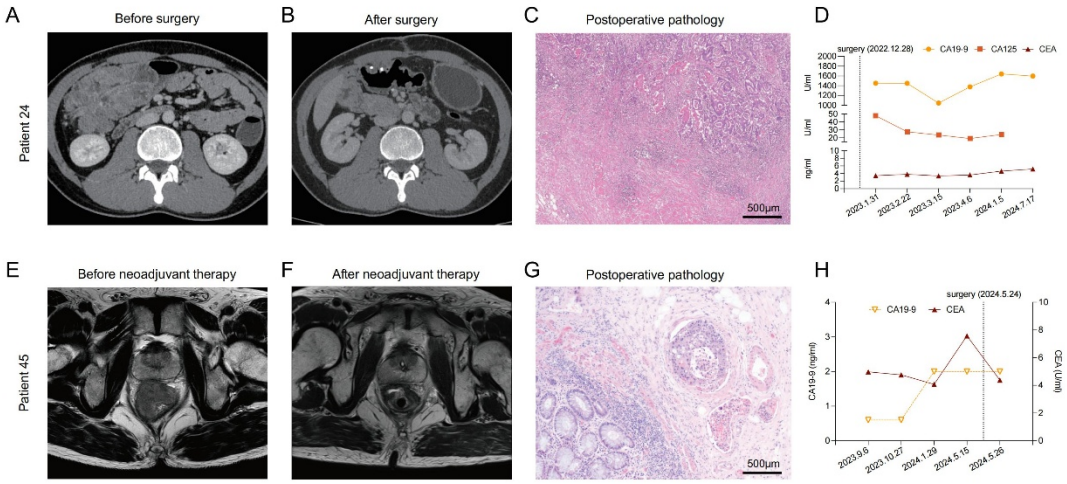

Extended Data Fig. 6 Longitudinal clinical imaging, pathological assessment, and tumor marker dynamics of representative CRASC patients

(A) Preoperative computed tomography (CT) scan of patient 24.

(B) Postoperative CT scan of patient 24.

(C) Histopathological analysis of tumor tissue from patient 24 following treatment.

(D) Longitudinal line plot depicting serum tumor marker levels (CEA, CA19-9 and CA125) during the treatment course of patient 24.

(E) Preoperative magnetic resonance imaging (MRI) scan of patient 45.

(F) Postoperative MRI scan of patient 45.

(G) Histopathological analysis of tumor tissue from patient 45 following treatment.

(H) Longitudinal line plot depicting serum tumor marker levels (CEA and CA19-9) during the treatment course of patient 45.